

The Calculation and Analysis of the Bistatic Quantum Radar Cross Section for the Typical 2-D Plate

Volume 10, Number 2, April 2018

Chonghua Fang

Hui Tan

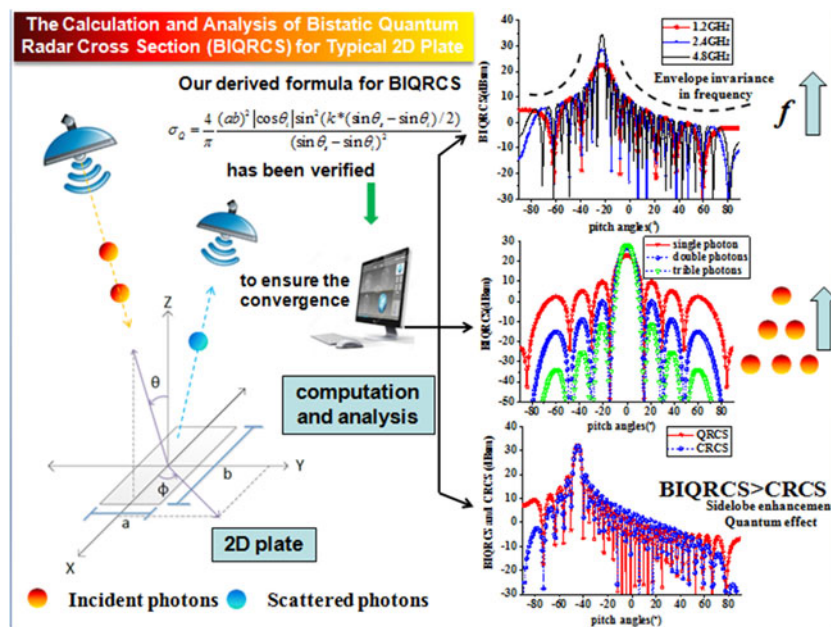
Qi-Feng Liu

Li Tao

Long Xiao

Yanjun Chen

Liang Hua



DOI: 10.1109/JPHOT.2018.2818819

1943-0655 © 2018 IEEE

The Calculation and Analysis of the Bistatic Quantum Radar Cross Section for the Typical 2-D Plate

Chonghua Fang^{1,2}, Hui Tan,¹ Qi-Feng Liu,¹ Li Tao,¹ Long Xiao,¹
Yanjun Chen,^{2,3} and Liang Hua^{2,4}

¹Science and Technology on Electromagnetic Compatibility Laboratory, China Ship Development and Design Centre, Wuhan 430000, China

²The Applied Electromagnetics Laboratory, University of Houston, Houston, TX 77081 USA

³College of Electronic Engineering, Xi'an Shiyou University, Xi'an 710065, China

⁴Institute of Technology, Zhejiang Business College, Hangzhou 310053, China

DOI:10.1109/JPHOT.2018.2818819

1943-0655 © 2018 IEEE. Translations and content mining are permitted for academic research only.
Personal use is also permitted, but republication/redistribution requires IEEE permission.
See http://www.ieee.org/publications_standards/publications/rights/index.html for more information.

Manuscript received February 7, 2018; revised March 15, 2018; accepted March 19, 2018. Date of publication March 23, 2018; date of current version April 6, 2018. This work was supported by the China Scholarship Council under Grant 201605280001; and in part by the National Natural Science Foundation of China under Grants 61601430 and 41474108. Corresponding author: C. Fang (e-mail: 27634073@qq.com).

Abstract: The quantum radar cross section (QRCS) describes how much return one gets when illuminating an object with a handful of photons. However, the previous studies mainly focused on the monostatic scattering of quantum radar. In this study, in response to the four key questions raised by ourselves in bistatic quantum radar cross section (BIQRCS), we calculate and analyze the BIQRCS for the typical tow-dimensional plate. First, as mentioned by Brandsema, the further derived analytical solution for the rectangular plate is obtained. In addition, the influence of incident frequency and the number of photons on the BIQRCS for the plate were obtained. Besides, we first reveal that the envelope curves of sidelobes in BIQRCS at the given incidence display the invariance in frequency. Finally, we show some comparison results among the BIQRCS, classical radar cross section (CRCS), and monostatic QRCS for the plate and find the advantage of sidelobe of the BIQRCS in given direction. We anticipate that these research results will find use in the detection and discrimination of stealthy platforms.

Index Terms: 2D plate, bistatic, calculation and analysis, quantum radar, quantum radar cross section.

1. Introduction

In recent years, quantum technology may prove especially useful in many scenarios too troublesome for conventional or classical systems [1]–[11]. In the field of detection and discrimination, any object reflects the signal to the detector, but the targets of low reflectivity immersed in regions with high background noise are hard to sense using classical systems. By contrast, quantum radars exploit quantum entanglement to enhance their sensitivity to detect and discriminate weak signals from very noisy surroundings. Further speaking, it seems that the quantum radar has another promising feature of enhanced side lobe target visibility in term of monostatic QRCS in comparison to the CRCS [12], [13]. According to the discoverer of this novel phenomenon [13], it could be regarded as a sort of quantum interference effect between the incident photon and the surface

atoms of the target. Afterwards, the development of related algorithm and theory help promote the progress in the field of quantum radar target scattering [14]–[27]. Among them, after ignoring diffraction and absorption effects, M. Lanzagorta took the lead in calculating and analyzing the QRCS properties under the influence of different sizes, incident frequencies and photons for the typical rectangular plate [13]. Then, the basic bistatic equations for 2D targets have already been derived by MJ Brandsema [14]. Meanwhile, he has also proposed a new framework form of the QRCS expression in terms of Fourier transforms for the typical two-dimensional (2D) targets. However, the most of previous studies were aimed at the monostatic scattering of quantum radar, a little information has focused on the calculation and analysis of bistatic scattering of that. Also, it's probably not very clear on the following questions.

- 1) Can we derive further the analytical solutions of bistatic scattering of quantum radar for the simple geometries followed the derivation of M. J. Brandsema, such as the rectangular plate?
- 2) What's the response of bistatic scattering under the influence of different frequencies, incident angles and photons?
- 3) What's the difference among the BIQRCS, CRCS and monostatic QRCS?
- 4) Whether there exists the similar sidelobe phenomenon in the bistatic scattering of quantum radar?

Although we believe that quantum radar can offer the prospect of detecting, identifying, and resolving radio frequency stealth platforms and weapons systems [13], there is short of taking full advantage of quantum radar without the answer to those issues.

This research aims to give the primary answers through a series of calculation and analysis on BIQRCS for the typical two-dimensional target, a rectangular plate. At first, followed the derivation of M. J. Brandsema, the analytical formula obtained in term of Fourier transforms is given for the rectangular plate. Moreover, the corresponding analytical results have a good agreement with the simulation data. In addition, the analysis of the BIQRCS responses as affected by different parameters is obtained. In the meanwhile, the analytical formula helps us understand that the envelope curves of sidelobes in BIQRCS at the given incidence display the invariance in frequency. Finally, we will also discuss the comparison of scattering properties among the BIQRCS, CRCS and monostatic QRCS.

2. Algorithm and Analytical Solution

2.1 Algorithm

The concept and expression of the quantum radar cross section (QRCS) have been introduced by [12], [13].

$$\sigma_Q = \lim_{R \rightarrow \infty} 4\pi R^2 \frac{\langle \hat{I}_s(\vec{r}_s, \vec{r}_d, t) \rangle}{\langle \hat{I}_i(\vec{r}_s, t) \rangle} \quad (1)$$

where \hat{I}_i and \hat{I}_s are the incident and scattered energy density of photons, respectively. \vec{r}_s , \vec{r}_d are the positions of the transmitter and the receiver, and R is the range from the quantum radar to the target.

In general, after ignoring diffraction and absorption effects, the simplified expression of QRCS for the case of the multiple-photon in the quantum radar pulse is given [14].

$$\sigma_Q = \frac{4\pi A_{\perp}(\theta_i, \Phi_i) \left| \sum_{n=1}^N e^{i(\vec{k}_i - \vec{k}_s) \bullet \vec{x}_n} \right|^{2M}}{\int_0^{2\pi} \int_0^{\pi/2} \left| \sum_{n=1}^N e^{i(\vec{k}_i - \vec{k}_s) \bullet \vec{x}_n} \right|^{2M} \sin \theta_s d\theta_s d\Phi_s} \quad (2)$$

where $A_{\perp}(\theta_i, \Phi_i)$ is the orthogonal projected area of the target in each incidence, N is the total number of illuminated atoms on the object's surface, \vec{k}_i and \vec{k}_s are the incident and scattered wave

vectors of the photon, \vec{x}_n is the position of the n th illuminated atom on the object's surface, θ_i and Φ_i are the incident angles of the photon impinging on the target and θ_s and Φ_s are the scattered angles, M is the number of incident photons in each pulse. As for the 2D plate, $A_{\perp}(\theta_i, \Phi_i) = A_{\perp\max} |\cos \theta_i|$, where $A_{\perp\max}$ is the cross sectional area of the plate at normal incidence. The absolute value ensures that the projected area is always positive [14].

2.2 Analytical Solution

This section presents the primary derivative process of the analytical solution of the rectangular plate and comparison with the simulation data. In the most common case that the object is not polarized, the surface atom density function $V(\vec{x}_n)$ becomes 1 on the surface of targets. Therefore, we can derive the analytical solution based on the following expression [14]:

$$\sigma_Q = \frac{4\pi A_{\perp}(\theta_i, \Phi_i) \left| \Gamma(V(\vec{x}_n)) \right|^{2M}}{\int_0^{2\pi} \int_0^{\pi/2} \left| \Gamma(V(\vec{x}_n)) \right|^{2M} \sin \theta_s d\theta_s d\Phi_s} \quad (3)$$

where $\Gamma(V(\vec{x}_n))$ represents the Fourier transform of $V(\vec{x}_n)$, and M represents the number of incident photons per pulse, \vec{x}_n is the position of the n th illuminated atom on the object's surface.

Further, we utilize this expression to achieve the closed-form solution for the simple geometry, such as the rectangular plate. For a 2D rectangular plate, of width a and height b , $\Gamma(V(\vec{x}_n))$ becomes the following [14]

$$\begin{aligned} \Gamma(V(\vec{x}_n)) &= \int_{-a/2}^{a/2} \int_{-b/2}^{b/2} e^{iK_x x + iK_y y} dx dy \\ &= \int_{-a/2}^{a/2} e^{iK_x x} dx \int_{-b/2}^{b/2} e^{iK_y y} dy \\ &= (ab) \frac{\sin(K_x a/2)}{K_x a/2} \frac{\sin(K_y b/2)}{K_y b/2} \end{aligned} \quad (4)$$

We have the following for the wave vector terms.

$$K_x = k(\sin \theta_s \cos \Phi_s - \sin \theta_i \cos \Phi_i) \quad (5)$$

$$K_y = k(\sin \theta_s \sin \Phi_s - \sin \theta_i \sin \Phi_i) \quad (6)$$

The basic bistatic equation has been shown to be [14]. Here, we'd like to examine the case of bistatic scattering further. For this scenario, the incident ray and the reflected ray are found in the same plane as usual. Meanwhile, since we defined the plate to be in the XOY plane, this means that to observe it at the principal angles, we can define $\Phi_i = \Phi_s = 0^\circ$ so that it should be a very typical case which is shown in Fig. 1. From these definitions, we have the following

$$K_x = k(\sin \theta_s - \sin \theta_i) \quad (7)$$

$$K_y = 0 \quad (8)$$

Accordingly, expression (4) further becomes

$$\Gamma(V(\vec{x}_n)) = \frac{(ab) \sin(ka(\sin \theta_s - \sin \theta_i)/2)}{ka(\sin \theta_s - \sin \theta_i)/2} \quad (9)$$

Moreover, for the 2D plate, this can be modeled satisfactorily by the following expression [14]:

$$A_{\perp}(\theta_i, \Phi_i) = A_{\perp\max} |\cos \theta_i| \quad (10)$$

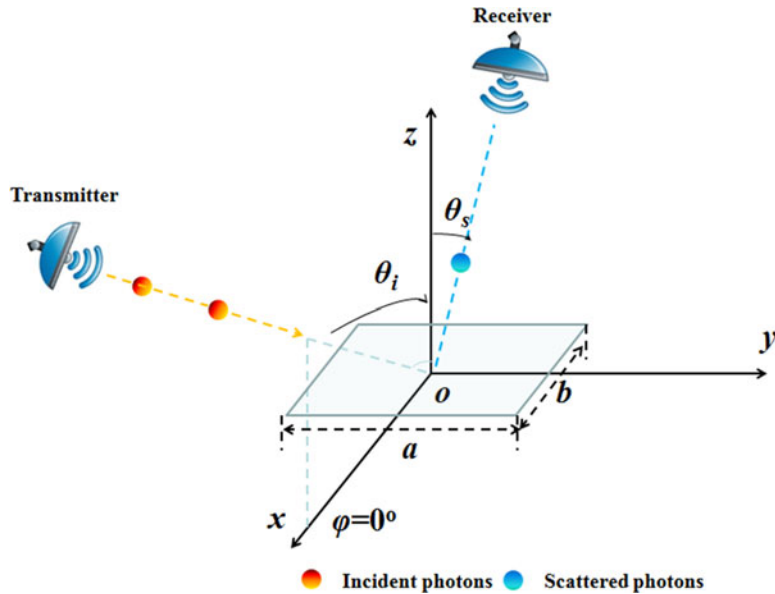


Fig. 1. The scenario of bistatic scattering and geometry of the rectangular plate.

Thus, the denominator term in (3) becomes $\lambda^2 ab \chi(k, a, b)$, where [14]

$$\chi(k, a, b) = \frac{(2\pi)^2 ab}{k^2} \left(\frac{1}{(2\pi)^2} \int_0^{\pi/2} \int_0^{2\pi} \frac{\sin^2(ka \sin \theta_s \cos \Phi_s/2)}{ka \sin^2 \theta_s \cos^2 \Phi_s/4} \frac{\sin^2(kb \sin \theta_s \sin \Phi_s/2)}{kb \sin^2 \theta_s \sin^2 \Phi_s/4} \sin \theta_s d\Phi_s d\theta_s \right) \quad (11)$$

We can set it to be approximately equal to 1 at high frequencies which means the target dimensions more than several wavelengths [14]. So, we can rewrite (3) as the following

$$\sigma_Q = \frac{4}{\pi} \frac{b^2 |\cos \theta_i| \sin^2(ka * (\sin \theta_s - \sin \theta_i)/2)}{(\sin \theta_s - \sin \theta_i)^2} \quad (12)$$

It is worth mentioning that referenced on what we have done, the similar BIQRCS expressions for other simple 2D geometries, such as the triangular and circle plates, could be derived. It might be the first closed-form solution of BIQRCS for the 2D plate. Besides, this solution can be used for a reference for comparison in the simulation and analysis.

For completeness, we now compare the simulation of the rectangular plate to the plot of (2) developed earlier. In addition, the number of scatterers used in the simulation has been enough to obtain an accurate large scattering angle response. As shown in Figs. 2–4, the theoretical curves match extremely well with the simulation plots.

3. Results

It is generally assumed that the scattering pattern for QRCS is a purely quantum mechanical effect due to quantum interference [13]. Next, let's show the variation behavior of the effect in the different cases. Like the simulation before them, the diffraction and absorption effects have been ignored. In this section, let us start with the simple case and change one variable at a time to observe how it affects the measured responses.

3.1 Different Electrical Sizes (Incident Frequencies)

In this section, we look at the simulated responses of a rectangular plate ($1 \text{ m} * 1 \text{ m}$) illuminated by a photon with the wavelengths of 0.25 m (1.2 GHz), 0.125 m (2.4 GHz) and 0.0625 m (4.8 GHz) per

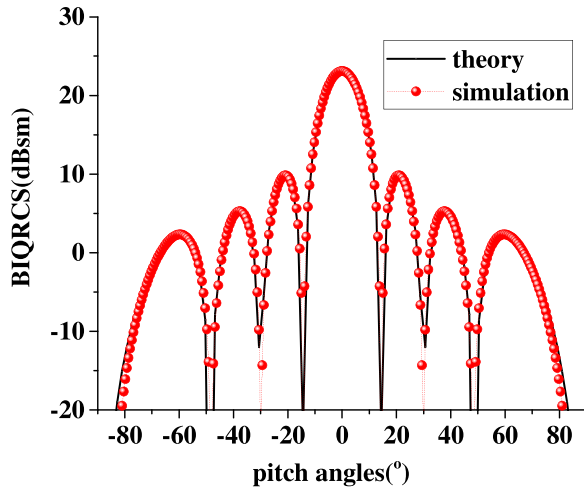


Fig. 2. Plots of the BIQRCS of theory and simulation for a $1\text{ m} * 1\text{ m}$ rectangular plate ($\theta_i = 0^\circ$, $\Phi_i = 0^\circ$).

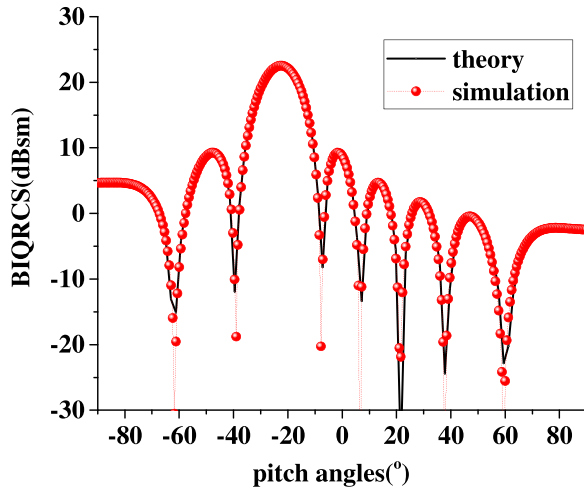


Fig. 3. Plots of the BIQRCS of theory and simulation for a $1\text{ m} * 1\text{ m}$ rectangular plate ($\theta_i = 22.5^\circ$, $\Phi_i = 0^\circ$).

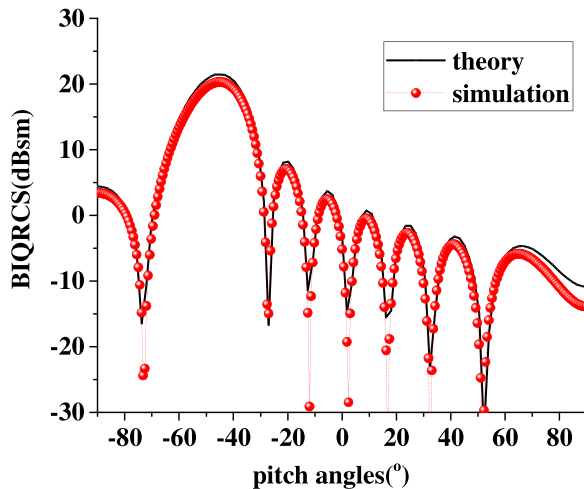


Fig. 4. Plots of the BIQRCS of theory and simulation for a $1\text{ m} * 1\text{ m}$ rectangular plate ($\theta_i = 45^\circ$, $\Phi_i = 0^\circ$).

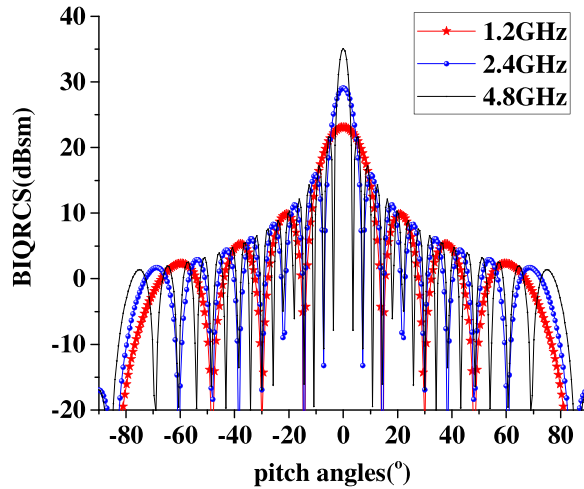


Fig. 5. Plots of the BIQRCS simulation for a 1 m * 1 m rectangular plate with different frequencies ($\theta_i = 0^\circ$, $\Phi_i = 0^\circ$).

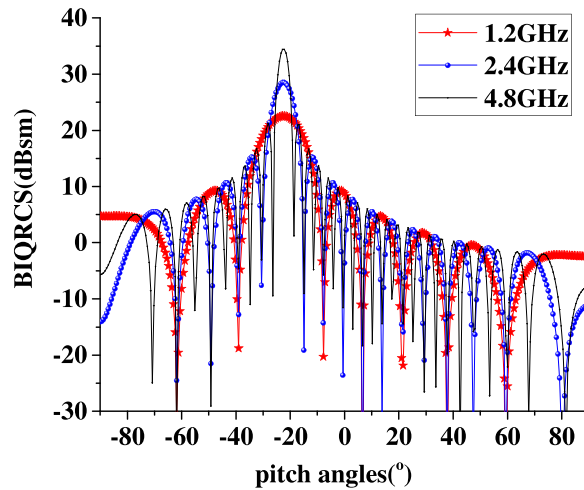


Fig. 6. Plots of the BIQRCS simulation for a 1 m * 1 m rectangular plate with different frequencies ($\theta_i = 22.5^\circ$, $\Phi_i = 0^\circ$).

pulse respectively. In other words, the side of the plate should be 4, 8, 16 wavelengths respectively. From the Figs. 5–7, we can see that with the increase of frequency, both the peak of main lobes and the number of nodes in the interference pattern go up accordingly. Moreover, as the incident photon is away from the normal of the plate, the corresponding scattering main lobes shift from the normal to the mirror symmetry directions. From these plots, however, it is also evident that the envelope curves of sidelobes are almost identical in each case of the same incidence with different frequencies. Meanwhile, It's still effective in what our calculation ability can afford, such as the case at 9.6 GHz.

Let's check the expression (12) and we can get more detail. To simplify the analysis, we can ignore the constant term and let the principal part of the expression, principal part = $\frac{|\cos \theta_i| \sin^2(ka * (\sin \theta_s - \sin \theta_i)/2)}{(\sin \theta_s - \sin \theta_i)^2}$, is divided into two parts, $part1 = \frac{|\cos \theta_i|}{(\sin \theta_s - \sin \theta_i)^2}$ and $part2 = \sin^2(ka * (\sin \theta_s - \sin \theta_i)/2)$. From the function curves of them in the Fig. 8 ($\theta_i = 0^\circ$, $\Phi_i = 0^\circ$), for example, we should clearly notice that the curve of part1 almost gives the envelope curve of the principal part of the expression while the curve of part2 mainly displays cyclic variations over the

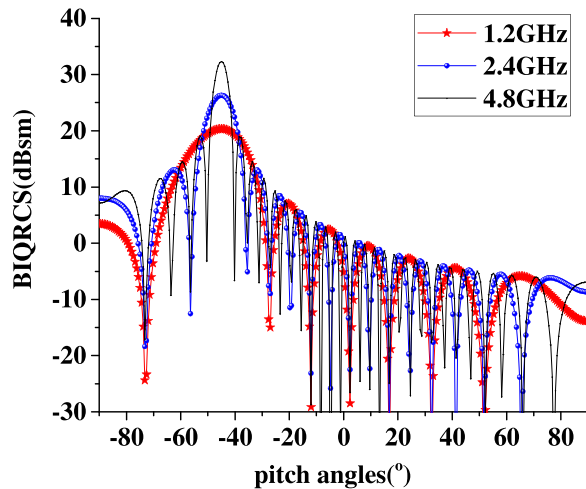


Fig. 7. Plots of the BIQRCS simulation for a $1 \text{ m} \times 1 \text{ m}$ rectangular plate with different frequencies ($\theta_i = 45^\circ$, $\Phi_i = 0^\circ$).

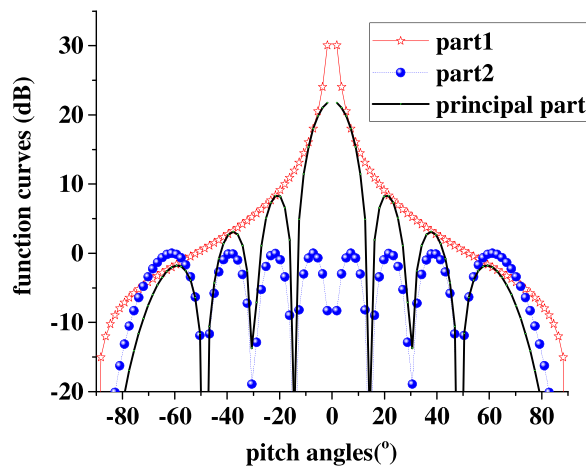


Fig. 8. Plots of function curves of the principal part, part1 and part2 of the expression (12) ($\theta_i = 0^\circ$, $\Phi_i = 0^\circ$). It should be noted that the values of three functions go to infinity at the point of $\theta_s = 0^\circ$ so that we ignore them in the figure.

pitch angles. As a result, due to the absence of k in the part1, the envelope curves of sidelobes in BIQRCS at the given incidence display the invariance in frequency.

3.2 Different Numbers of Incident Photons

Figs. 9–11 show the plots of BIQRCS with the incidences of one, two, and three photons in each pulse at different incident angles (for a rectangular target made of $1 \text{ m} \times 1 \text{ m}$), respectively. It can be observed that as the number of photons increases, so does the peaks of the maximum value of BIQRCS at each mirror symmetry directions while the width of the main lobe become more narrow. Moreover, the sidelobe structure decreases markedly and the peak of the lateral lobes appears to decrease exponentially faster with the number of photons. Therefore, it may be well worth considering if it is possible to detect stealthy targets using the main lobe of bistatic quantum radars operating at each mirror symmetry directions in the small photon number regime.

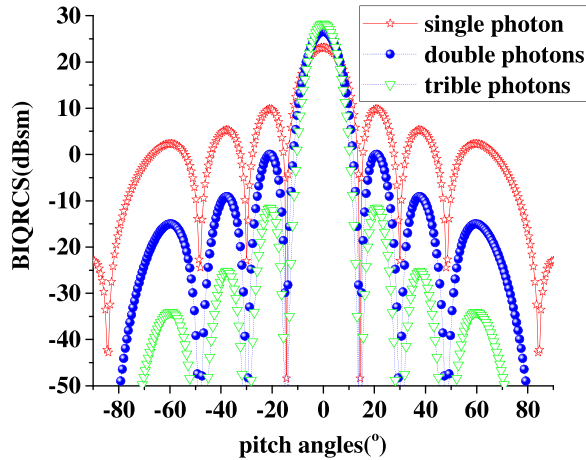


Fig. 9. BIQRCS responses of a rectangular plate of size 1 m * 1 m, illuminated with 1-3 photons in each pulse, respectively ($\theta_i = 0^\circ$, $\Phi_i = 0^\circ$).

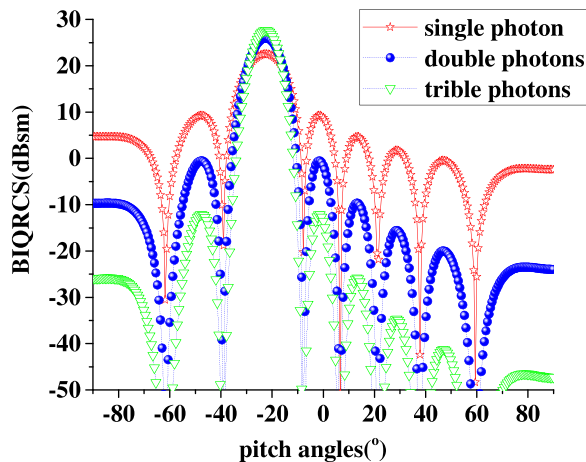


Fig. 10. BIQRCS responses of a rectangular plate of size 1 m * 1 m, illuminated with 1-3 photons in each pulse, respectively ($\theta_i = 22.5^\circ$, $\Phi_i = 0^\circ$).

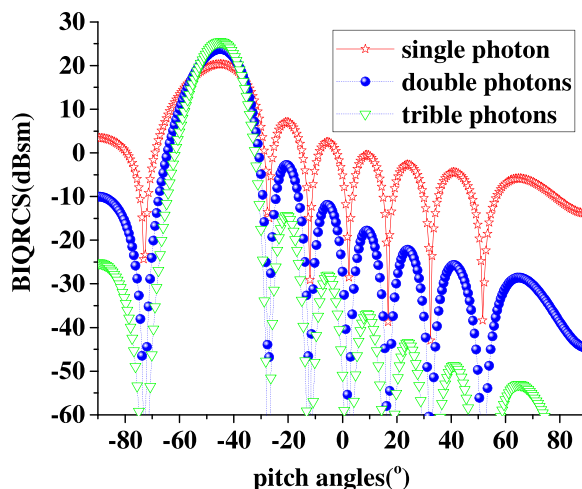


Fig. 11. BIQRCS responses of a rectangular plate of size 1 m * 1 m, illuminated with 1-3 photons in each pulse, respectively ($\theta_i = 45^\circ$, $\Phi_i = 0^\circ$).

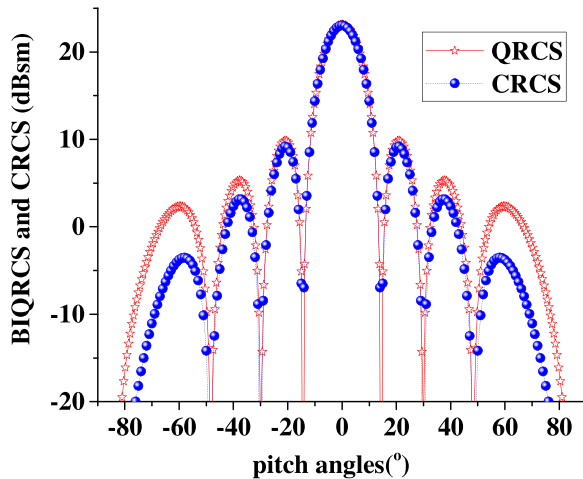


Fig. 12. BIQRCS and CRCS responses of a rectangular plate of size $1\text{ m} * 1\text{ m}$, illuminated with 1 photon with the frequency of 1.2 GHz, respectively ($\theta_i = 0^\circ$, $\Phi_i = 0^\circ$).

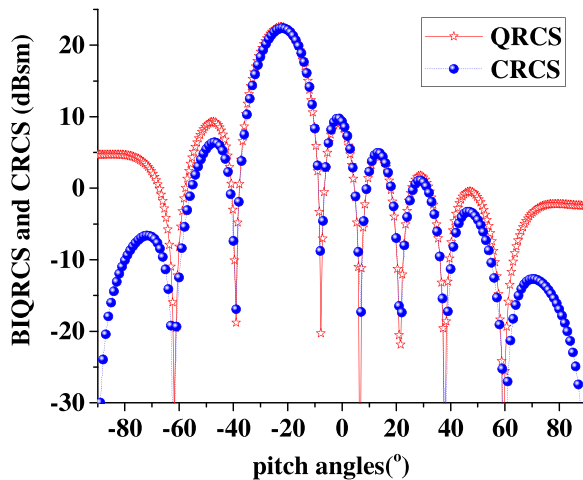


Fig. 13. BIQRCS and CRCS responses of a rectangular plate of size $1\text{ m} * 1\text{ m}$, illuminated with 1 photon with the frequency of 1.2 GHz, respectively ($\theta_i = 22.5^\circ$, $\Phi_i = 0^\circ$).

3.3 Comparison With CRCS

In this section, we will use the physical optics (PO) by the electromagnetic computing tool (FEKO) to calculate the bistatic CRCS data. Within the limits of pitch angle ($0\text{--}45^\circ$), this BIQRCS sidelobe advantage can be clearly observed by comparing the two kinds of plots in Figs. 12–20. Besides, it tends to be remarkable with the increasing of incident frequency. With the deviation of incidence from the normal of the plate, the advantage of sidelobe structure tends to increase in a whole. In fact, due to the specular reflection, the scattering energy usually mainly distributes in the direction of mirror symmetry, so does the nearby angle domains on the side of main lobes. Relatively speaking, the main lobes are almost the same values, respectively. Therefore, other than the directions of main lobes, it seems that it may be useful to detect the stealthy targets in the larger receiving pitch angle domain.

3.4 Comparison With MonoQRCS

As for the special case of monostatic QRCS, we expect that the BIQRCS expression (12) will become the expression of monostatic QRCS, namely MonoQRCS, in [14]. At this time, due to the

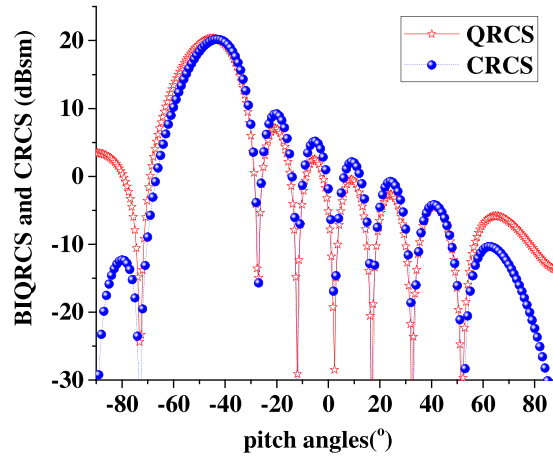


Fig. 14. BIQRCS and CRCS responses of a rectangular plate of size $1\text{ m} * 1\text{ m}$, illuminated with 1 photon with the frequency of 1.2 GHz, respectively ($\theta_i = 45^\circ$, $\Phi_i = 0^\circ$).

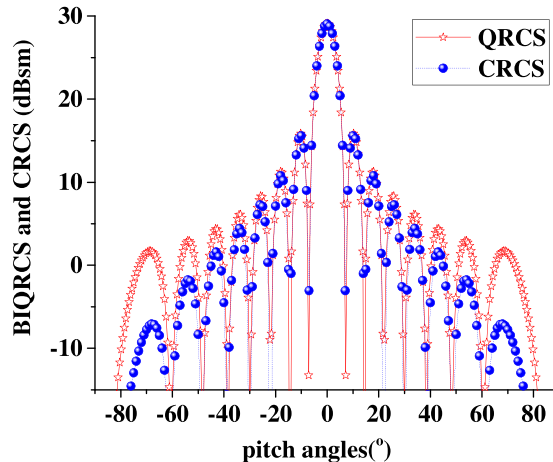


Fig. 15. BIQRCS and CRCS responses of a rectangular plate of size $1\text{ m} * 1\text{ m}$, illuminated with 1 photon with the frequency of 2.4 GHz, respectively ($\theta_i = 0^\circ$, $\Phi_i = 0^\circ$).

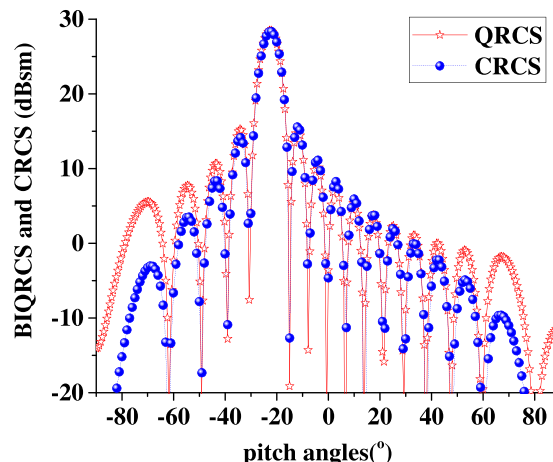


Fig. 16. BIQRCS and CRCS responses of a rectangular plate of size $1\text{ m} * 1\text{ m}$, illuminated with 1 photon with the frequency of 2.4 GHz, respectively ($\theta_i = 22.5^\circ$, $\Phi_i = 0^\circ$).

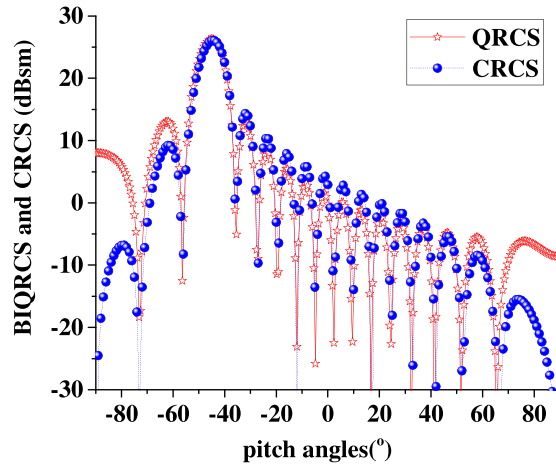


Fig. 17. BIQRCS and CRCS responses of a rectangular plate of size $1\text{ m} \times 1\text{ m}$, illuminated with 1 photon with the frequency of 2.4 GHz, respectively ($\theta_i = 45^\circ$, $\Phi_i = 0^\circ$).

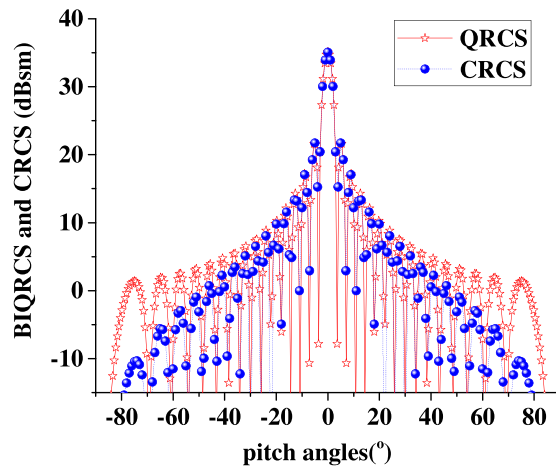


Fig. 18. BIQRCS and CRCS responses of a rectangular plate of size $1\text{ m} \times 1\text{ m}$, illuminated with 1 photon with the frequency of 4.8 GHz, respectively ($\theta_i = 0^\circ$, $\Phi_i = 0^\circ$).

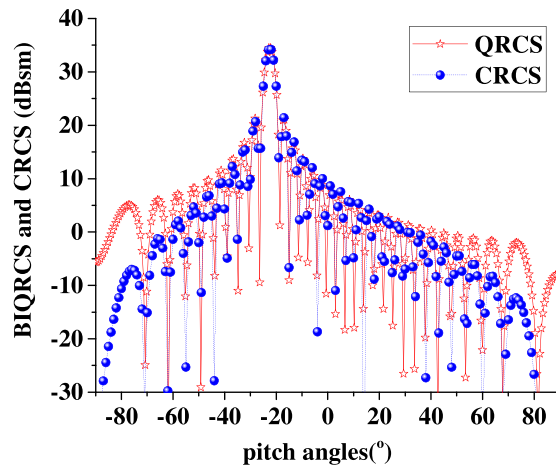


Fig. 19. BIQRCS and CRCS responses of a rectangular plate of size $1\text{ m} \times 1\text{ m}$, illuminated with 1 photon with the frequency of 4.8 GHz, respectively ($\theta_i = 22.5^\circ$, $\Phi_i = 0^\circ$).

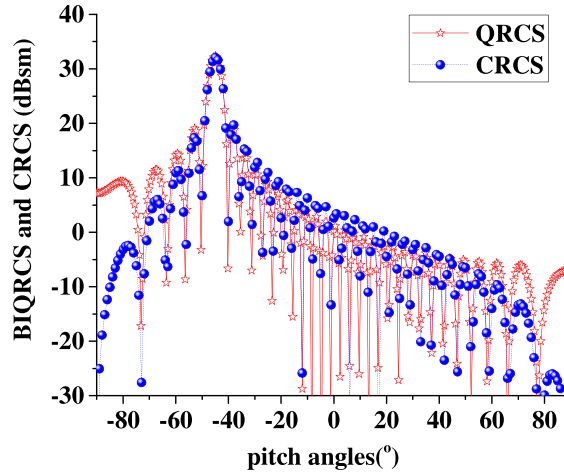


Fig. 20. BIQRCS and CRCS responses of a rectangular plate of size $1 \text{ m} * 1 \text{ m}$, illuminated with 1 photon with the frequency of 4.8 GHz , respectively ($\theta_i = 44.5^\circ$, $\Phi_i = 0^\circ$).

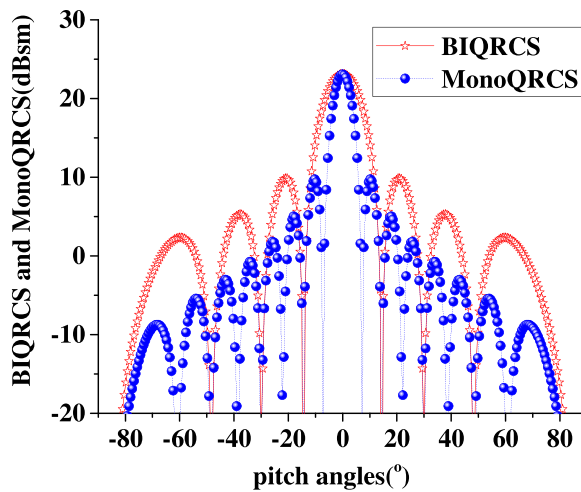


Fig. 21. MonoQRCS and BIQRCS ($\theta_i = 0^\circ$, $\Phi_i = 0^\circ$) responses of a rectangular plate of size $1 \text{ m} * 1 \text{ m}$, illuminated with single photon with the frequency of 1.2 GHz , respectively.

relationship $\theta_i = -\theta_s$ for the case of MonoQRCS, we can rewrite the BIQRCS expression (12) as the following item,

$$\begin{aligned}\sigma_{MQ} &= \frac{4}{\pi} \frac{b^2 |\cos \theta_i| \sin^2(ka * \sin \theta_i)}{(2 \sin \theta_i)^2} \\ &= \frac{k^2 a^2}{\pi} \frac{b^2 |\cos \theta_i| \sin^2(ka * \sin \theta_i)}{(ka * \sin \theta_i)^2} \\ &= \frac{k^2 a^2}{\pi} \frac{b^2 |\cos \theta_i| \sin^2(ka * \sin \theta_i)}{(ka * \sin \theta_i)^2} \\ &= \frac{4\pi a^2 b^2}{\lambda^2} |\cos \theta_i| \left(\frac{\sin(ka * \sin \theta_i)}{ka * \sin \theta_i} \right)^2\end{aligned}$$

So, we can safely obtain the expression of monostatic QRCS derived by M. J. Brandsema [14] from our formula. Further, in order to investigate the difference between the BIQRCS and MonoQRCS, we

have selected the cases of normal incidence ($\theta_i = 0^\circ$) which is relatively representative to analysis the difference.

Besides, from expressions (12) and of MonoQRCS, we note that the BIQRCS expression contains a $|\sin \theta_s/2|$ term, while the MonoQRCS expression contains a $|\sin \theta_s|$ term. This can be observed by comparing curves of the two curves in Fig. 21.

A natural question arises as to what causes the BIQRCS to be proportional to $|\sin \theta_s/2|$ and the MonoQRCS to be proportional to $|\sin \theta_s|$. In fact, it is obvious to see that both two items emerge from the items of K_x in expression (5).

4. Conclusion

Bistatic quantum radar is a potentially powerful technique for performing detection and discrimination, in which the scattering properties may offer more selections. In this study, a closed-form solution of BIQRCS has been derived from Fourier transforms of QRCS expression for the rectangular plate. In addition, the solution has been verified by the simulation data. Besides, our results indicate that with the increase of frequency, both the peak of main lobes and the number of nodes in the BIQRCS pattern go up accordingly. Meanwhile, we first reveal that the envelope curves of sidelobes in BIQRCS at the given incidence display the invariance in frequency. Further, it may be well worth considering the results may be useful to detect the stealthy targets with bistatic quantum radars using the sidelobe in the larger receiving pitch angle domain with single-photon illumination. Alternatively, one can use the main lobe at each mirror symmetry directions in the small photon number regime. Eventually, we have obtained the comparison results among BIQRCS, CRCS and monostatic QRCS for the plate. Meanwhile, it is worth mentioning that we have used the assumptions of ignoring diffraction and absorption effects. To confirm the results of these calculation and analysis results more completely, an ingenious verifying test based on the faint laser system, such as a single photon source, is suggested for further studies.

Acknowledgment

The authors would like to thank the anonymous reviewers for their valuable suggestions.

References

- [1] E. D. Lopatova, I. Ruo Berchera, S. Olivares, G. Brida, I. P. Degiovanni, and M. Genovese, "A detailed description of the experimental realization of a quantum illumination protocol," *Phys. Scr.*, vol. T160, Nov. 2014, Art. no. 14026.
- [2] E. D. Lopatova, I. R. Berchera, I. P. Degiovanni, S. Olivares, G. Brida, and M. Genovese, "Experimental realisation of quantum illumination," *Phys. Rev. Lett.*, vol. 110, no. 15, 2013, Art. no. 153603.
- [3] K. Jiang, H. Lee, C. C. Gerry, and J. P. Dowling, "Super-resolving quantum radar: Coherent-state sources with homodyne detection suffice to beat the diffraction limit," *J. Appl. Phys.*, vol. 114, no. 19, Nov. 2013, Art. no. 193102.
- [4] S. Barzanjeh, S. Guha, C. Weedbrook, D. Vitali, J. H. Shapiro, and S. Pirandola, "Microwave quantum illumination," *Phys. Rev. Lett.*, vol. 114, no. 8, 2015, Art. no. 080503.
- [5] S. Lloyd, "Quantum Illumination," *Science*, vol. 321, 2008, Art. no. 1463.
- [6] B. Xiong, X. Li, X. Y. Wang, and L. Zhou, "Improve microwave quantum illumination via optical parametric amplifier," *Ann. Phys.*, vol. 385, pp. 757–768, 2017.
- [7] Y. Nakamura and T. Yamamoto, "Breakthroughs in Photonics 2012: Breakthroughs in microwave quantum photonics in superconducting circuits," *IEEE Photon. J.*, vol. 5, no. 2, Nov. 2013, Art. no. 701406.
- [8] M. Sanz, U. Las Heras, J. J. García-Ripoll, E. Solano, and R. Di Candia, "Quantum estimation methods for quantum illumination," *Phys. Rev. Lett.*, vol. 118, Nov. 2017, Art. no. 070803.
- [9] U. Las Heras, R. Di Candia, K. G. Fedorov, F. Deppe, M. Sanz, and E. Solano, "Quantum illumination unveils cloaking," *Sci. Rep.*, vol. 7, 2017, Art. no. 9333.
- [10] U. Las Heras, R. Di Candia, K. G. Fedorov, F. Deppe, M. Sanz, and E. Solano, "Quantum illumination reveals phase-shift inducing cloaking," *Sci. Rep.*, vol. 7, no. 1, 2017, Art. no. 9333.
- [11] S. Lloyd, "Enhanced sensitivity of photodetection via quantum illumination," *Science*, vol. 321, no. 5895, pp. 1463–1465, 2008.
- [12] M. Lanzagorta, "Quantum radar cross section," *Proc. SPIE*, vol. 7727, 2010, Art. no. 77270K.
- [13] M. Lanzagorta, *Quantum Radar*, San Rafael, CA, USA: Morgan & Claypool, 2011.
- [14] M. J. Brandsema, "Formulation and analysis of the quantum radar cross section," *Ph.D. dissertation*, Dept. Elect. Eng., Pennsylvania State Univ., State College, PA, USA, 2017.
- [15] M. Malik and R. W. Boyd, "Quantum imaging technologies," *Rivista del Nuovo Cimento*, vol. 37, no. 5, pp. 1–3, 2014.

- [16] K. Liu, H. Xiao, H. Fan, and Q. Fu, "Analysis of quantum radar cross section and its influence on target detection performance," *IEEE Photon. Technol. Lett.*, vol. 26, no. 11, pp. 1146–1149, Jun. 2014.
- [17] K. Liu, H. Xiao, H. Fan, and Q. Fu, "Analysis and simulation of quantum radar cross section," *Chin. Phys. Lett.*, vol. 31, no. 3, Jan. 2014, Art. no. 034202.
- [18] C. Kun, C. Shuxin, W. Dewei, W. Xi, and S. Mi, "Analysis of quantum radar cross section of curved surface target," *Acta Optica Sinica.*, vol. 36, no. 12, Dec. 2016, Art. no. 1227002.
- [19] M. J. Brandsema, R. M. Narayanan, and M. Lanzagorta, "Theoretical and calculational analysis of the quantum radar cross section for simple geometrical targets," *Quantum Inf. Process.*, vol. 16, no. 1, pp. 1–27, 2017.
- [20] Y. Lin, L. Guo, and K. Cai, "An efficient algorithm for the calculation of quantum radar cross section of flat objects," in *Proc. Int. Symp. Progr. Electromagn. Res.*, 2014, pp. 39–43.
- [21] K. Liu, Y. Jiang, X. Li, Y. Cheng, and Y. Qin, "New results about quantum scattering characteristics of typical targets," in *Proc. Int. Symp. Geosci. Remote Sens.*, Nov. 2016, pp. 2669–2671.
- [22] M. Lanzagorta and S. Venegas-Andraca, "Algorithmic analysis of quantum radar cross sections," *Proc. SPIE*, vol. 9461, May 2015, Art. no. 946112.
- [23] M. J. Brandsema, R. M. Narayanan, and M. Lanzagorta, "Cross section equivalence between photons and non-relativistic massive particles for targets with complex geometries," *Progr. Electromagn. Res. M*, vol. 54, pp. 37–46, 2017.
- [24] M. J. Brandsema, R. M. Narayanan, and M. Lanzagorta, "Electric and magnetic target polarization in quantum radar," *Proc. SPIE*, vol. 10188, May 2017, Art. no. 101880C.
- [25] S.-L. Xu, Y.-H. Hu, N.-X. Zhao, Y.-Y. Wang, L. Li, and L.-R. Guo, "Impact of metal target's atom lattice structure on its quantum radar cross-section," *Acta Phys. Sin.*, vol. 64, no. 15, Jan. 2015, Art. no. 154203.
- [26] C. Fang, "The simulation and analysis of quantum radar cross section for three-dimensional convex targets," *IEEE Photon. J.*, vol. 10, no. 1, Feb. 2018, Art. no. 7500308.
- [27] C. H. Fang, "The simulation of quantum radar scattering for 3D cylindrical targets," in *Proc. 2018 Int. Conf. IEEE Calculational Electromagn.*, pp. 978–980, 2018.